[UCI]I804:21031-200000291217

Thesis for the Degree of Master of Engineering

Photoluminescence Properties of Dy^{3+} Ions Doped in $Gd_{10}V_2O_{20}$ Vanadate

by

Shala Bi

Interdisciplinary Program of

Biomedical, Mechanical & Electrical Engineering

The Graduate School

Pukyong National University

February 2020

Photoluminescence Properties of Dy^{3+} Ions Doped in $Gd_{10}V_2O_{20}$ Vanadate

(Dy^{3+} 이온이 첨가된 바나듐산염 $Gd_{10}V_2O_{20}$ 형광체의 형광특성)

Advisor: Prof. Hyo Jin Seo

by

Shala Bi

A thesis submitted in partial fulfillment of the requirements for the degree of

Doctor of Engineering

in Interdisciplinary Program of Biomedical, Mechanical & Electrical Engineering, The Graduate School,

Pukyong National University

February 2020

Luminescence Properties of Dy^{3+} Ions Doped in $Gd_{10}V_2O_{20}$ Vanadate

A dissertation

by

Shala Bi

Approved by:

_____

(Chairman: Prof. Cheol Woo Park)

_____ _____

(Member: Ph.D. Kyoung Hyuk Jang) (Member: Prof. Hyo Jin Seo)

February 2020

Content

List of Figures

Photoluminescence Properties of Dy^{3+} Ions Doped in $Gd_{10}V_2O_{20}$ Vanadate

Shala Bi

Interdisciplinary Program of Biomedical, Mechanical & Electrical Engineering, The Graduate School,
Pukyong National University

Abstract

A series of Dy^{3+} doped $Gd_{10}V_2O_{20}$ phosphors were synthesized by the high-temperature solid state reaction at 1200 ℃. The crystal structure, morphology, and luminescence properties are investigated. The phase purity of the samples is confirmed by the X-ray diffraction analyses. The concentration-dependent luminescence properties are studied in the range from 0 to 70 mol % under the ultraviolet excitation at 355 nm, which shows the optimum doping concentration is 3 mol %. The $Gd_{10}V_2O_{20}$ phosphor shows strong emission intensity at 575 nm, which is assigned to the spin-forbidden transition of $^4F_{9/2} \rightarrow {}^6H_{13/2}$. Temperature-dependent emission spectra were recorded under the 266 nm excitation in the temperature range from 10 to 480 K. The decay curves of Dy^{3+} ions in the $Gd_{10}V_2O_{20}$ lattices are also studied. The emission intensity ratio of $^4F_{9/2} \rightarrow {}^6H_{15/2}$ (blue, 482 nm) and $^4F_{9/2} \rightarrow {}^6H_{13/2}$ (yellow, 572 nm) and phosphor thermal sensitivity of $Gd_{10}V_2O_{20}$:Dy^{3+} are systematically investigated.

Dy^{3+} 이온이 첨가된 바나듐산염 $Gd_{10}V_2O_{20}$ 형광체의 형광특성

Shala Bi

부경대학교 대학원 의생명기계전기융합공학협동과정

요 약

1200 ℃의 고온 고상 법으로 Dy^{3+} 이온이 도핑 된 $Gd_{10}V_2O_{20}$ 형광물질을 합성하여 형광특성을 연구하였다. 결정구조와 결정상은 X선 회절 분석으로 확인하였다. 355 nm의 자외선으로 시료를 여기 하였으며 Dy^{3+} 이온의 농도는 0 ~ 70 mol % 이었다. 이 중 최적 도핑 농도는 3 mol%임을 확인하였다. $Gd_{10}V_2O_{20}$:Dy^{3+}가 방출하는 가장강한 형광은 $^4F_{9/2} \rightarrow {}^6H_{13/2}$ 스핀금지 전이에 의한 황색 575 nm 형광 이었으며 다음이 $^4F_{9/2} \rightarrow {}^6H_{15/2}$ 전이에 의한 청색 482nm 형광이었다. 온도 범위 10 ~ 480 K에서 온도 의존 형광특성 및 형광의 동역학 특성을 조사하였다. 575 nm 형광의 수명 시간은 농도가 1.0에서 70 mol %까지 증가하는 동안 153에서 20 μs까지 짧아졌다. Dy3+ 이온의 농도와 온도 변화에 따른 형광특성 변화를 조사하였다. 특히 청색 형광 482 nm 와 황색 형광 575 nm 의 상대적 변화를 체계적으로 조사하였다.

1. Background

Solid state lighting (SSL) is a new technology used to generate artificial white light by using semiconductor diode (LEDs) which produce light in the visible range with the following of electric current inside the diode (electroluminescence). SSLs are mainly categorized in to three major groups according to the semiconducting materials used for its manufacturing, which are the polymer, organic and inorganic light emitting diodes [1].

1.1. Introduction to luminescence

The essence of luminescence is the conversion of energy, that is, the process of converting absorbed energy into light energy. Luminescence has two basic features:[2] (1) it is unbalanced radiation superimposed on the basis of thermal radiation, and after the material absorbs the external energy, it emits a portion of the total radiation that exceeds the equilibrium radiation (thermal radiation). (2) When the external excitation source stops the excitation of the material, the emission process will continue for a while, which is the "afterglow phenomenon". Fluorescence is generally less than 10^{-8} s, and phosphorescence is greater than 10^{-8} s.

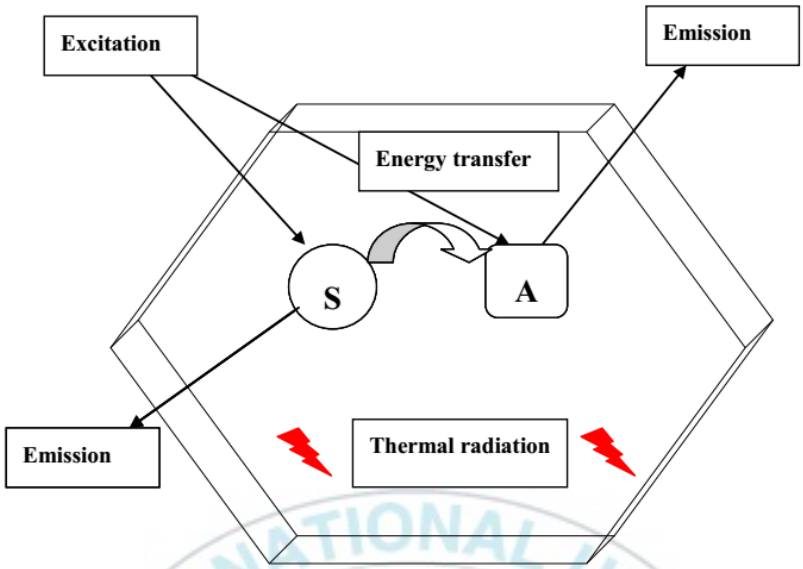

Figure 1-1 The main physical process of luminescence, M: matrix; S: sensitizer; A: activator; in the matrix.

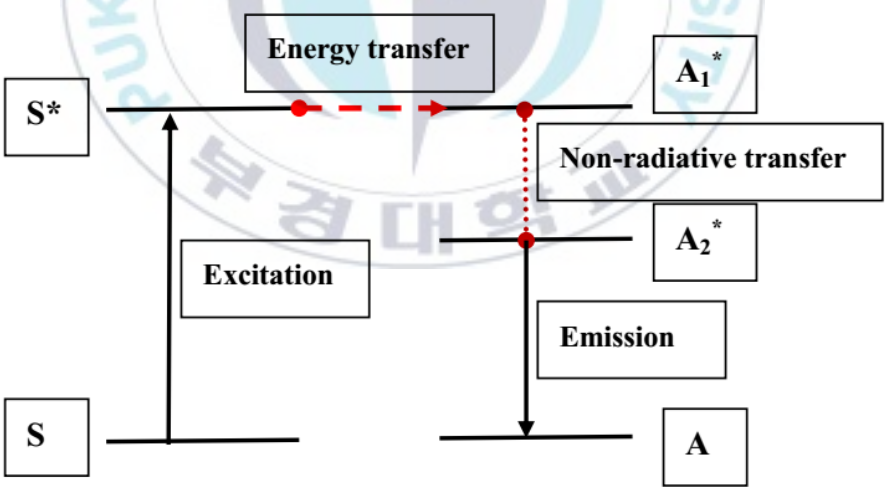

Figure 1-2 The energy transfer from sensitizer to activator, S: ground state of sensitizer; S*: excited state of sensitizer; A: ground state of activator; A1*, A2*: excited state of activator.

The main physical processes in the luminescence process include the following steps:

A. When the material is excited by an external excitation source, both the matrix lattice and the luminescent center absorb certain energy.

B. Matrix pass absorbed energy to activate the agent A, make the activator of the outermost electron transition from the ground state to the excited state, stay electronics from the excited state to ground state, will release energy in the form of radiation, which produces light. In addition, after absorbing energy matrix, can produce electronic - hole pair in the matrix, the electron and hole could be migrated and bound on the luminescence center, while the electrons return to ground state or electrons and holes of the composite will release energy in the form of light.

C. The sensitizer S transfers the absorbed energy to the activator A in whole or in part by means of energy transfer, thereby enhancing the energy absorption of the activator, thereby improving the luminous efficiency.

D. When the electron is excited to transition to the excited state, the final return to the ground state will also be accompanied by a part of the non-radiative transition, the energy is lost in the form of heat, and fluorescence quenching occurs, which will result in a decrease in luminous efficiency.

1.1.1. Working principle and history of a light emitting diode

White light emitting diodes, also named as White LEDs, a new lighting source is composed of light emitting diode and phosphor which can be effectively excited by the light emitting diode. White LED greatly exceeds the luminous efficiency of traditional lighting systems, bringing new functions to lighting systems and greatly enhancing the way we use light. The significant advantages and great application prospect of white LED to make it the research focus of the world.

The first light emitting diode reported in the literature was formed by a Russian scientist Oleg Vladimirovich Losev in the year of 1927. After the word war, most of the attention is diverted to the infrared light emitting diodes, prominently developing of gallium arsenide (GaAs) [3]. In 1962, an American scientist Nick Holonyak Jr developed for the first time a practical light emitting diode that has the emission in the visible region (red light). Gallium arsenide phosphate (GaAsP) is a new developed light emitting diode (LED) which emit a poor red light which works up to milli-Ampere current [4]. At last at the year of 1992, the brightness blue light emitting diode (GaN) was formed by Shuji Nakamura of Nichia Corporation. The present technology improved to a great extent after then, which wok with nearly one Ampere current are common nowadays. The development of gallium nitride (GaN) brings an outstanding scientific advancement in the field of the light emitting diode. Before the development of GaN, the bright light emitting diodes were only achievable for

the emitting range of yellow to infrared. The discovery of GaN leads the research to achieve blue, green and white light emitting diodes (LEDs).

1.1.2. Advantages of white light emitting diodes

Compared with traditional lighting sources, the white LED has some obvious advantage, as follows:

- Fast switching, can reach nanoseconds, high color rendering index (CRI>80);
- Can be used for an extensive of correlated color temperatures (2700 K-6000 K);
- No ultraviolet and infrared radiation causes fading of colored objects;
- Wide operating temperature range (-20 ^{o}C-85 ^{o}C);
- No pollution and safety, environmentally friendly properties;
- White LEDs are not harmful to the environment during production and use. chemicals that eliminate the pollution of mercury Hg to the human body and the surrounding environment;
- High luminous efficiency (the year 2014: about 140 lm/W; the future is expected to 2020 exceed by 200 lm/W);
- Low energy loss, low voltage (<4 V);
- Low current (<700 mA);
- Long lifetime: white LEDs can last up to tens of thousands of hours and are the longest life source;
- No filament blowing problem;

- Lumen efficiency can still be maintained above 70% after prolonged use;
- Wide spectral range, white light LED spectral range can cover the entire visible region;
- Small size, lightweight, can be made into an array or wrappable components, easy to design;

Light source	Mechanism	Light effect /m/W	CRI	Color Temp /K	Life expectancy/h
Incandescent lamp	Thermal luminescence	15	100	2800	1000
High pressure mercury lamp	Aerial discharge	50	45	3300-4300	6000
Tricolor fluorescent lamp	Aerial discharge	93	80-98	All series	12000
LED	Electron complex luminescence	140	>80	2700-6000	25000-50000

Table 1-1 The comparisons of main technical indicators between w-LEDs and another light source

1.1.3. White light emitting diodes implementation

White LEDs can be used as general lighting devices, so they are attracted much attention. In general, there are three options for using LED chips to make white light, are as follows:

1) Three primary colors of light emitted by three red, green, and blue

monochromatic LED chips are mixed to generate white light.

2) By adjusting the mixing ratio of the three primary colors of red, green and blue phosphors, three kinds of phosphors are simultaneously excited by ultraviolet, near ultraviolet or blue LED chips, and red, green and blue light are combined to obtain white light.

3) A yellow phosphor is coated on the blue LED chip, and the blue light emitted by the chip is complementarily mixed with the yellow light emitted by the phosphor to form white light.

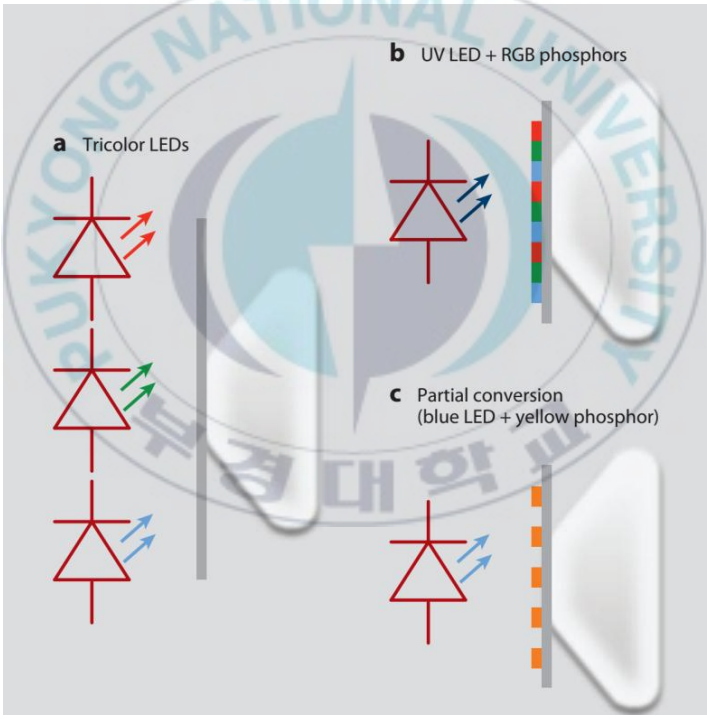

Figure 1-3 Three methods of generating white light. (1) red + green + blue-LEDs; (2) UV-LED + RGB phosphors; (3) blue-LED + yellow phosphor.

1.2. Light emission mechanism in rare earth doped phosphor

1.2.1. 4f-4f transitions

In the trivalent Re^{3+} doped phosphors, the 4f-4f electronic transition is prominent in which 4f electrons are moved between various levels of energy of the same rare earth ions[5]. This type of electronic transitions is parity forbidden according to the selection rules of parity, which pronounce that the transition of electrons cannot occur between those energy levels which have the same parity[6]. hence the energy levels of the 4f orbital have similar parity, therefore its 4f-4f electronic transition is forbidden. Actually, this transition is occurring due to the relaxation produced in the form of electron vibrations and an unbalanced crystal field applied from the phosphors host[7].

However in the trivalent ions of lanthanide series, the 4f electrons are shield by the 5s and 5p electrons from the extrinsic fields, therefore the effect of the host crystal field on it is negligible. Therefore, every trivalent lanthanide ions are individually characterized by its own energy levels independent from the effect of host materials, therefore the 4f-4f transition provides a narrow absorption and emission band, as shown in Figure 1-4.

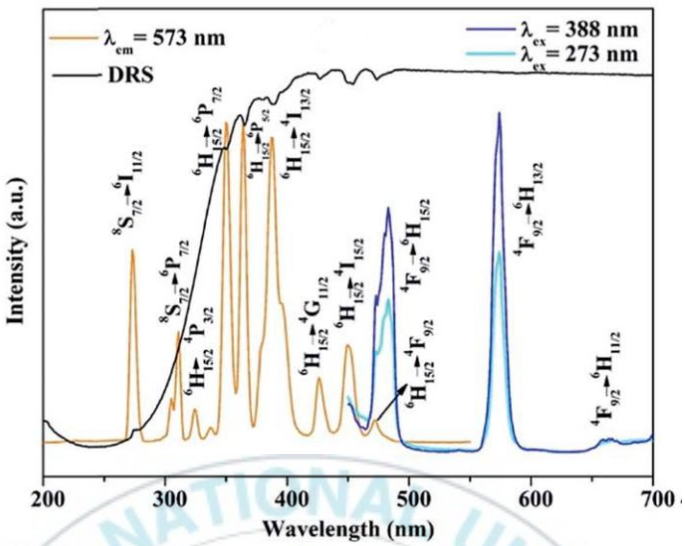

Figure 1-4 The PLE and PL spectra, and UV-vis DRS of $K_2Gd(PO_4)(WO_4)$:0.005Dy^{3+}.

It is clearly seen that in the diagram that the excitation spectrum is a narrow band ranging from 200 nm to 500 nm have a maximum peak at 355 nm. In the PLE spectrum, two sharp bands at 273 and 313 nm are from $^8S_{7/2}$ - $^6I_{11/2}$ and $^8S_{7/2}$ - $^6P_{7/2}$ transitions of Gd^{3+} ions, respectively. Other bands at 324, 350, 364, 388, 426, 450 and 472 nm are originating from $^6H_{15/2}$ - $^4P_{3/2}$, $^6H_{15/2}$ - $^6P_{7/2}$, $^6H_{15/2}$ - $^6P_{5/2}$, $^6H_{15/2}$ - $^4I_{13/2}$, $^6H_{15/2}$ - $^4G_{11/2}$, $^6H_{15/2}$ - $^4I_{15/2}$, and $^6H_{15/2}$ - $^4F_{9/2}$ f-f transitions of Dy^{3+} ions[8].

Dieke and his co-worker made this trivalent rare earth-transition identification in the 1960s[9], their diagram (Dieke diagram) shown in Fig. 1-5 used to identify transitions which are based on their own energies.

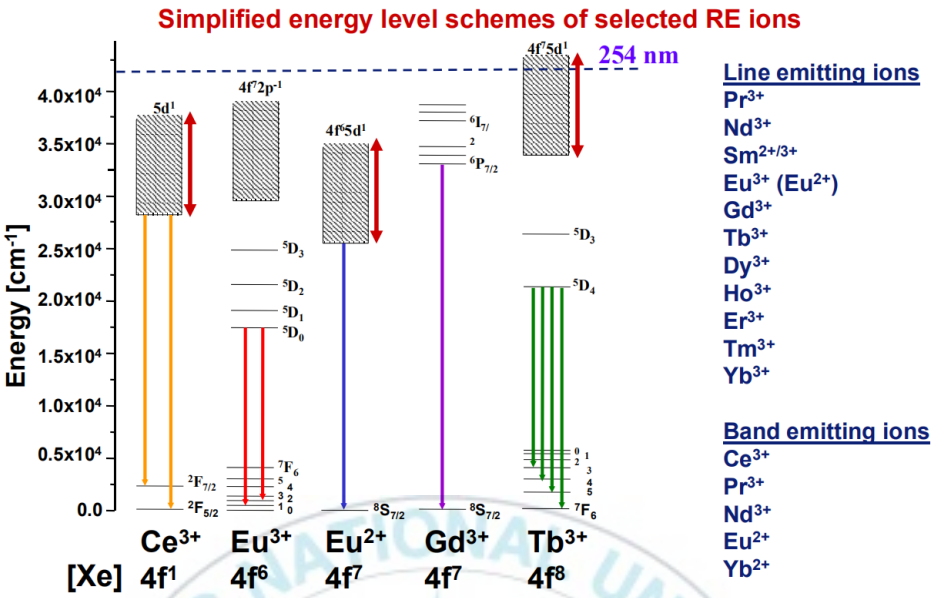

Figure 1-5 Energy levels diagram of the free trivalent ions of the lanthanide series [8].

1.2.2. 4f-5d transitions

A multiple numbers of divalent and trivalent rare earth ions, such as Eu^{2+}, Ce^{3+}, Er^{3+}, and Pr^{3+}, which can be directly excited from the 4f ground state having $4f^n$ configuration to a 5d excited state having $4f^{n-1}d^1$ configuration which can be either emit through 4f-4f intra band transition or a 5d-4f transition. However, unlike to the transitions of the multiple states of the $4f^n$ configuration that is strongly forbidden with the selection rule, the transitions from 4f to 5d are allowed the transition. Moreover unlike to the 4f state that is independent from the effect of outside crystal field effect of the host, the 4f to 5d transition are strongly dependent on the crystal field effect and vary over a long spectral range that is from UV to infrared region, because the 5d states of the activators are diffused and well overlap with the orbital of ligand[10].

Fig. 1-7 presents the schematics affect of the host lattice crystal field on the activator energy state that is the $4f^7$ and $4f^65d^1$ of the divalent Eu^{2+} ions[10]. Fig. 1-6 clearly illustrate that the emission of the activators changes from the UV line emission to the band emission of the visible light region by increasing the effect of the host lattice crystal field.

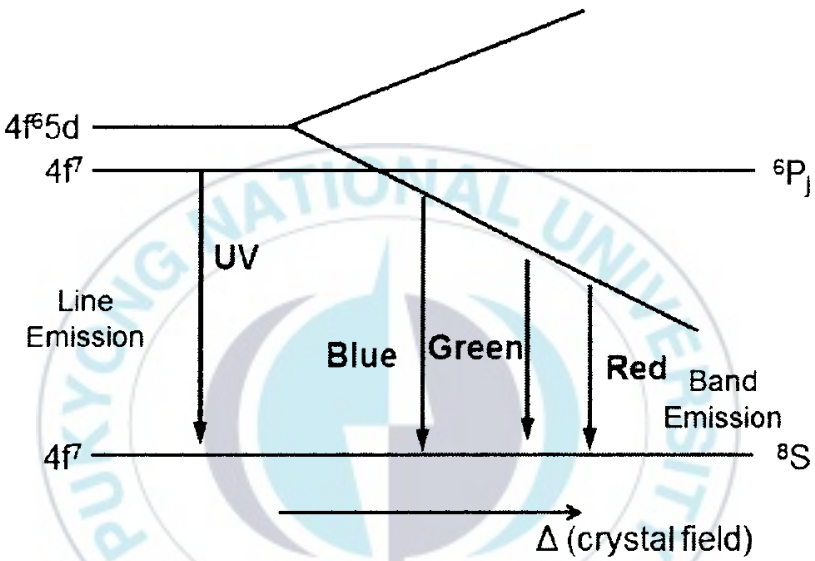

Figure 1-6 The schematics effect of the host crystal field on the 4f-5d energy level of the divalent Eu^{2+} ions.

Therefore it is to be more liked that to search a host in which the 4f-5*d* transitions of the activator leads to an absorption spectra cover the UV, near UV or blue region and having the respective emission in the visible range (430 nm to 700 nm). the activator candidates having this type of transition are divalent Eu^{2+} and trivalent Ce^{3+} ions[10]. That is why the maximum of the phosphors used for the application of light emitting diode having these two ions as activators.

1.2.3. Luminescence properties of the Dy^{3+} ions

Dysprosium ions (Dy^{3+}) is a single-doped matrix that produces white-emitting rare earth activator ions. the luminescence lines of Dy^{3+} are in the 470 to 500 nm region due to the $^4F_{9/2}\rightarrow{}^6H_{15/2}$ transition, the $^4F_{9/2}\rightarrow{}^6H_{15/2}$ transition is a magnetic dipole transition[11-14], which is less affected by the crystal field environment; And in the 570 to 600 region duo to the $^4F_{9/2}\rightarrow{}^6H_{13/2}$ transition. the $^4F_{9/2}\rightarrow{}^6H_{13/2}$ transition is an ultra-sensitive transition of the electric dipole, which is greatly affected by the crystal field environment. Achieved by adjusting the intensity ratio of yellow light to blue light, the color of the luminescence is close to white[15].

A lot of research shows, there are two, three or four emission peaks in the emission spectrum of Dy^{3+} ion-activated luminescent materials, which are located at about 485, 575, 660 and 755 nm. The blue emission around 485 nm is attributed to the transition from $^4F_{9/2}\rightarrow{}^6H_{15/2}$, the yellow-green emission around 575 nm is attributed to the transition from $^4F9/2\rightarrow{}^6H_{13/2}$, the red emission around 660 nm is attributed to the transition from $^4F_{9/2}\rightarrow{}^6H_{11/2}$, and the brownish red emission around 775 nm is attributed to the transition from $^4F_{9/2}\rightarrow{}^6H_{9/2}$[16-18]. Figure 1-7 shows energy level diagram of Dy^{3+} ions. Dy^{3+}-activated white luminescent materials have low preparation cost, appropriate color rendering index and related color temperature, great thermal stability and chemical stability, and high quantum efficiency, they have broad application prospects as potential single-phase white light emitting phosphors.

1.3. Scopes and outline of this thesis

The aims of this study are to design novel Dy^{3+} and Sm^{3+} rare earth ion doped phosphors and investigate the optical properties and their application in optical temperature sensing. This general will be described as the following:

In Chapter 2, we introduce a novel Dy^{3+}-activated $Gd_{10}V_2O_{20}$ Vanadate phosphor, which has been successfully synthesized by a solid-state method and suggests Dy^{3+} doped phosphors as optical thermometry materials. The Dy^{3+} excitation and emission spectroscopy techniques were used to analyze the luminescence properties of phosphors and to determine the crystallographic position of Dy^{3+} in the phosphor matrix. Measurement the dependence of the luminescence properties and decay time of Dy^{3+} on temperature, and acquaintance the thermal stability of phosphors.

In Chapter 3, we proposed a novel white light emitting phosphor $Gd_{10}V_2O_{20}$:Dy^{3+} codoped with Sm^{3+}, to improving the color-rendering index (Ra) owing to a red component contribution.

Finally, Conclusions and summary are listed.

2. Synthesis and Luminescence Properties of color-tunable Dy^{3+}-activated $Gd_{10}V_2O_{20}$ phosphor

2.1. Introduction

Recently, the trivalent RE ion, dysprosium (Dy^{3+}), has drawn much attention due to its unique photoluminescence (PL) emission and potential application in optical temperature sensors[19]. Generally, Dy^{3+} ions have two dominant emission bands in the blue (460-500 nm) and yellow (560-600 nm) regions. The blue emission corresponding to $^4F_{9/2}$ - $^6H_{15/2}$ transition is the magnetic transition, which is insensitive to the local environment, whereas the yellow emission corresponding to $^4F_{9/2}$ - $^6H_{13/2}$ transition is the hypersensitive electric dipole transition ($\Delta L=2$, $\Delta J=2$) and its intensity is strongly affected by the crystal field around Dy^{3+} ions. Therefore, the color-tunable emissions are expected to be realized in Dy^{3+} ions doped materials by changing the yellow-to-blue intensity ratio[20]. Guo et al. reported that the emission color of the Dy^{3+}-activated $Li_8Bi_2(MoO_4)_7$ phosphors can be changed from yellow to white through modifying the Y/B ratio[21]. Furthermore, Liu et al. also demonstrated that the emission color of Dy^{3+} activated $NaY(WO_{4)2}$ phosphors can be tuned from greenish blue to yellowish green[21]. It is noted that most of the studies on the color-tunable emissions of Dy^{3+} ions were mainly carried out either by adjusting the Dy^{3+} ion concentration or choosing different host lattices. However, there are few investigations on the excitation wavelength dependent emission.

In this paper, the Dy^{3+}-activated $Gd_{10}V_2O_{20}$ phosphors were synthesized by the high-temperature solid-state method. The photo-luminescence (PL) properties,

ET mechanism between Dy^{3+} ions in $Gd_{10}V_2O_{20}$ phosphors, and chromatic properties were investigated. The PL properties at different temperature were also analyzed.

2.2. Experimental Section

2.2.1. Sample preparation

Dy^{3+} doped $Gd_{10}V_2O_{20}$ with various Dy^{3+} concentrations of x=0, 0.01, 0.02, 0.03, 0.05, 0.07, 0.1, 0.15, 0.2, 0.3, 0.5 and 0.7 were synthesized via the high-temperature solid-state method. The specific operation steps are as follows:

A. Raw material is weighted

Turn on the electronic balance and preheat for a few minutes, after the electronic balance is stabilized, according to the appropriate stoichiometric ratio, the starting materials, Gd_2O_3 (Aldrich, 99.9%), V_2O_5 (Aldrich, 99.9%), Dy_2O_3 (Aldrich, 99.9%).

B. mixture the starting materials

All the starting reagents were mixed in stoichiometric ratios and ground in an agate mortar to obtain the homogeneous mixture.

C. Previous calcining

Starting reagents were grounded thoroughly in an agate mortar with ethanol, the mixture was calcined at 600 ℃ for 6 h in a crucible in the atmosphere, and then cooling to room temperature.

D. Ground and calcination again

After cooling to room temperature, grounded thoroughly again in an agate mortar with ethanol, then the homogenous mixture was calcined at 1200 ℃ for 12 h in a crucible in the atmosphere. Thus, a series of the xDy^{3+} doped $Gd_{10}V_2O_{20}$ phosphors were successfully obtained as cooling down to room temperature.

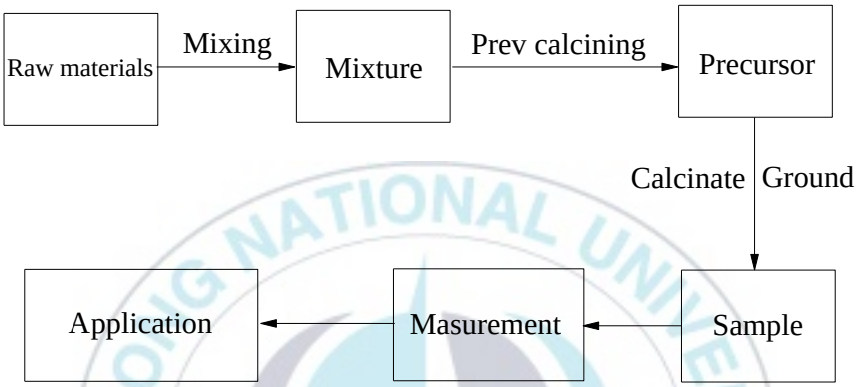

Figure 2-1 The preparation process of the high-temperature solid-state method

2.2.2. Characterization

In this work, the crystal phases of the $Gd_{10}V_2O_{20}$:Dy^{3+} samples were identified by using an X-ray Rigaku D/Max diffractometer(XRD) operating at 40 kV, 30 mA equipped by Cu $K\alpha$ radiation (λ= 1.5405 Å). A 450 W Xe lamp dispersed by a 25 cm monochromator (Acton Research Corp. Pro-250) was used as a light source for excitation and emission spectra. The luminescence signal was detected using a photomultiplier tube (PMT) (Hamamatsu, R928, Shizuoka, Japan) mounted on a 75 cm monochromator (Acton Research Corp. Pro-750). The third

harmonic (266 nm or 355 nm) of a pulsed Nd: YAG laser was introduced as an excitation source for luminescence decays which were digitized and saved by means of a 500 MHz Tektronix DPO 3054 oscilloscope. For low-temperature measurements, the samples were placed in a closed-cycle helium cryostat in the variable-temperature range (7 - 300 K).

2.3. Results and Discussion

2.3.1. Morphology and composition

Figure 2-2 shows the XRD patterns of Dy^{3+} co-doped $Gd_{10(1-x)}V_2O_{20}$ (x=0, 0.01, 0.02, 0.03, 0.05, 0.07, 0.1, 0.15, 0.2, 0.3, 0.5 and 0.7) samples synthesized by high-temperature solid-state reaction method. Which are well indexed to the standard card (PDF # 22-0296) without any impurities phases. No evident peak shift in the XRD patterns is observed even at Dy^{3+} content of 70% indicating the introduction of activated Dy^{3+} impurities does not cause significant changes to the crystallinity.

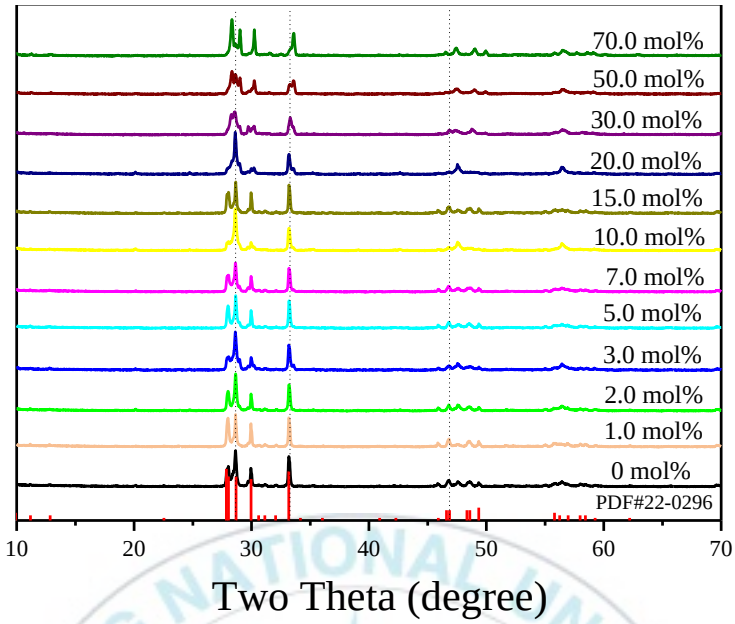

Figure 2-2 XRD patterns of $Gd_{10}V_2O_{20}$:x% Dy^{3+} (x = 0-70) and the PDF standard card

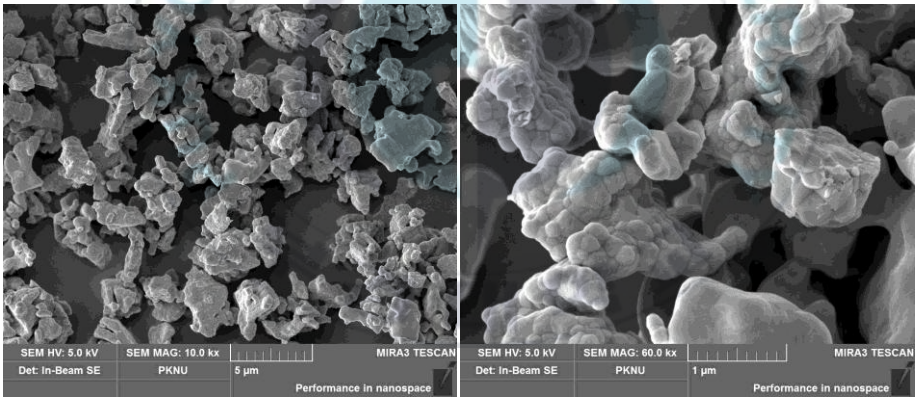

Figure 2-3 Typical granular morphology of $Gd_{10}V_2O_{20}$:0.05Dy^{3+} with the size distribution in the range of 5 μm and 1 μm

The scanning electron microscopy (SEM) image of a representative sample is shown in Figure 2-3, exhibiting irregular distribution-like morphology with a particle size of about 1 um.

2.3.2. Emission, excitation spectra and decay curves

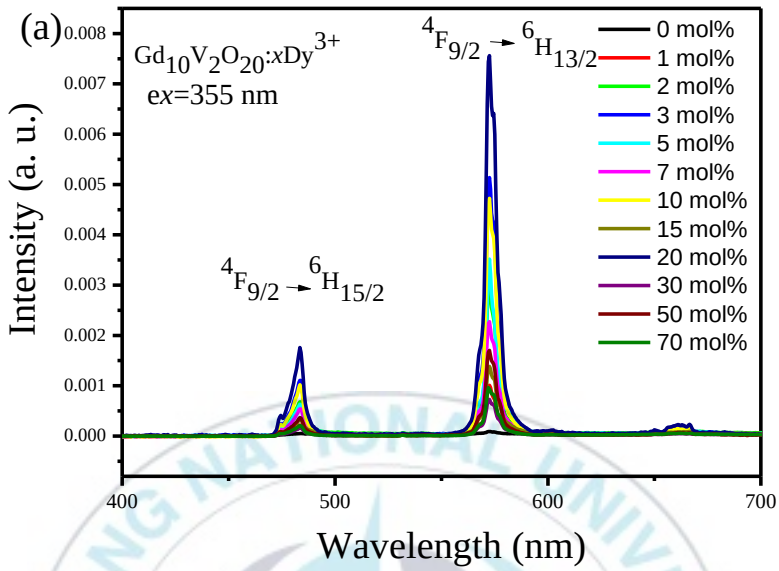

Figure 2-4 PL emission spectra of the Gd10V2O20:x Dy3+ (x=0, 0.01, 0.02, 0.03, 0.05, 0.07, 0.1, 0.15, 0.2, 0.3, 0.5 and 0.7) phosphors excited at355 nm.

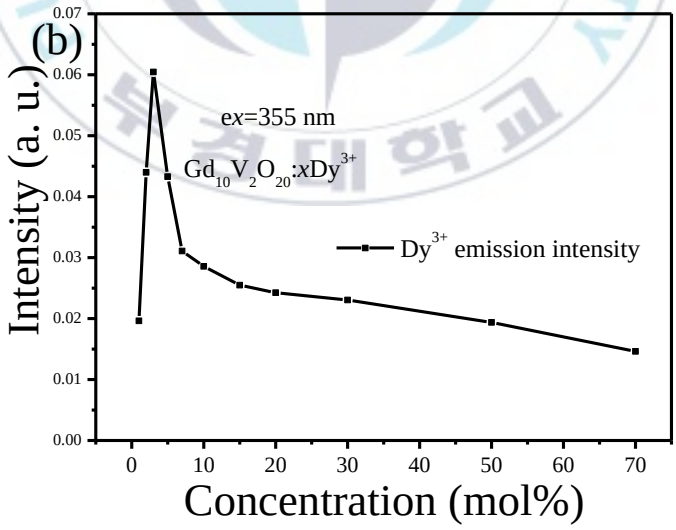

Figure 2-5 Intensity of $Gd_{10}V_2O_{20}$:x Dy^{3+} (x=0, 0.01, 0.02, 0.03, 0.05, 0.07, 0.1, 0.15, 0.2, 0.3, 0.5 and 0.7) phosphors with different Dy^{3+} doping concentration.

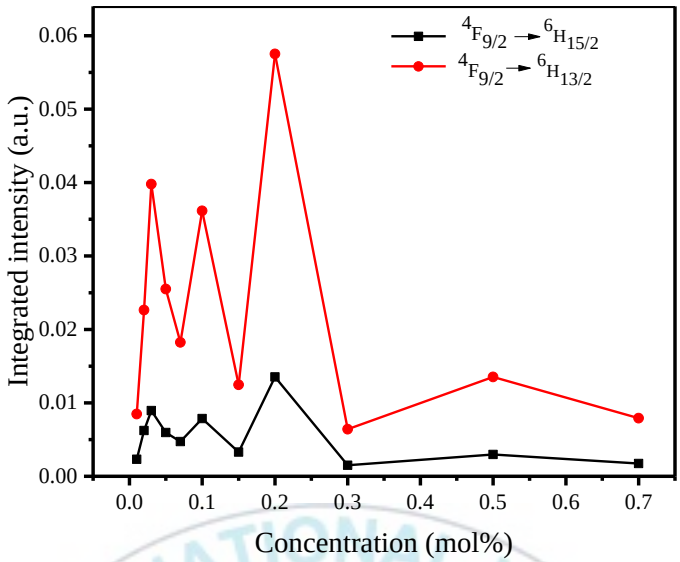

Figure 2-6 Two emission peaks integral ratio of $Gd_{10}V_2O_{20}$:*x* Dy^{3+} (*x*=0, 0.01, 0.02, 0.03, 0.05, 0.07, 0.1, 0.15, 0.2, 0.3, 0.5 and 0.7) phosphors emission intensity with different Dy^{3+} doping concentration.

The PL emission spectra of Dy^{3+}-activated $Gd_{10}V_2O_{20}$ phosphors for different Dy^{3+} ion concentrations at an excitation wavelength of 355 nm are shown in Figure 2-5 It is found that the PL profiles were similar and the position of emission peaks did not vary with the Dy^{3+} ion concentration. However, the intensity of each emission increased gradually with increasing the Dy^{3+} ion concentration, which reaches its maximum value when *x*=0.03. Then, the intensity decreased with further increment of Dy^{3+} ion concentration owing to the concentration quenching caused by the resonant ET between Dy^{3+} ions.

Figure 2-6 shows the integral ratio of $Gd_{10}V_2O_{20}$:*x* Dy^{3+} (*x*=0, 0.01, 0.02, 0.03, 0.05, 0.07, 0.1, 0.15, 0.2, 0.3, 0.5 and 0.7) phosphors emission intensity with different concentrations.

The luminescence decay time of the phosphor means that the time interval

between the phosphor excitation and the detection of emitted the light. There are two common forms of attenuation, exponential decay, and non-exponential decay.

(1) Exponential decay

Where I_0 is the luminous intensity at the moment of excitation stop,t is time, τ is the decay lifetime, the τ is the time at which the luminescence intensity is reduced to 1/*e* times its initial intensity. In a discrete luminescence center system, the luminescence intensity I(t) after the termination of excitation with a short pulse follows the exponential function formula:[1]

$$I(t) = I_0 \exp(-t/\tau) \qquad (2\text{-}1)$$

(2) Non-exponential decay

Where t is time, I(t) is the luminous intensity at t time after the excitation cutoff, and $\tau_{average}$ is the average decay lifetime. Generally, the non-exponential decay occurs when the thermal activation energy migrates during the luminescence.

$$\tau_{average} = \frac{\int_0^\infty I(t)tdt}{\int_0^\infty I(t)dt} \qquad (2\text{-}2)$$

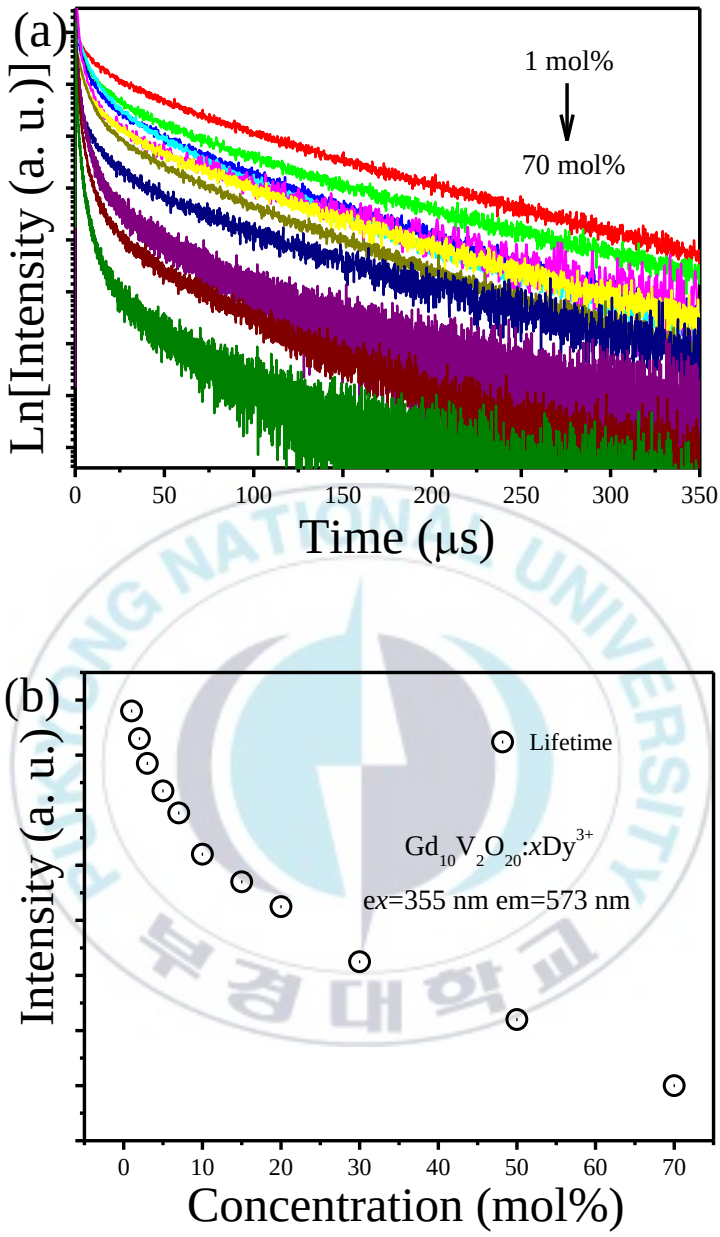

Figure 2-7 The decay curves of $Gd_{10}V_2O_{20}$:*x* Dy^{3+} (*x*=0, 0.01, 0.02, 0.03, 0.05, 0.07, 0.1, 0.15, 0.2, 0.3, 0.5 and 0.7) phosphors (λ*ex* = 355 nm) (λ*em* = 573 nm) and **(b)** lifetimes of phosphors with different Dy^{3+} doping concentration

Figure 2-7 shows the PL decay curves of the $^4F_{9/2}$-$^6H_{13/2}$ transition for the $Gd_{10}V_2O_{20}$:*x* Dy^{3+} (*x*=0, 0.01, 0.02, 0.03, 0.05, 0.07, 0.1, 0.15, 0.2, 0.3, 0.5 and 0.7) phosphors under 266 nm of excitation wavelength and 572 nm of emission wavelength. It is clear that the decay curves revealed a single exponential shape that can be well fitted by the above expression. From **Eq. (2-2)**, the t_0 values for *x*= 0.01, 0.03, 0.05, 0.07, 0.1, 0.15, 0.2, 0.3, 0.5 and 0.7 were estimated to be about 153, 145, 140, 122, 100, 98, 92, 88, 80, 72 and 20 μs (see **Figure 2-7**), respectively. It is evident that the lifetime decreased slightly with the increment of Dy^{3+} ion concentration upto *x*=0.05, and then decreased sharply with further increment of Dy^{3+} ions concentration due to the concentration quenching.

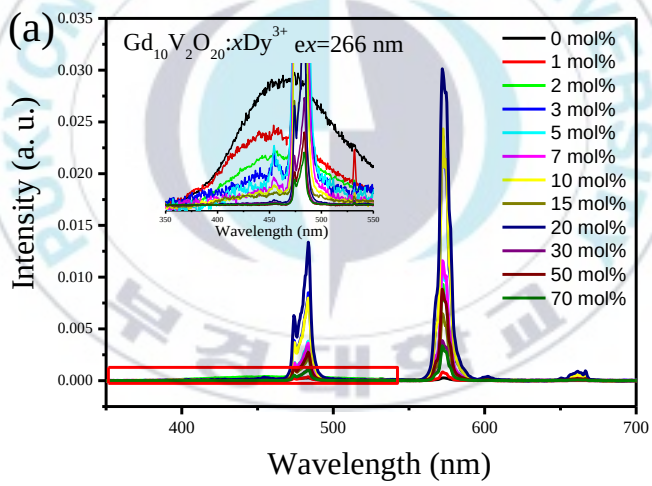

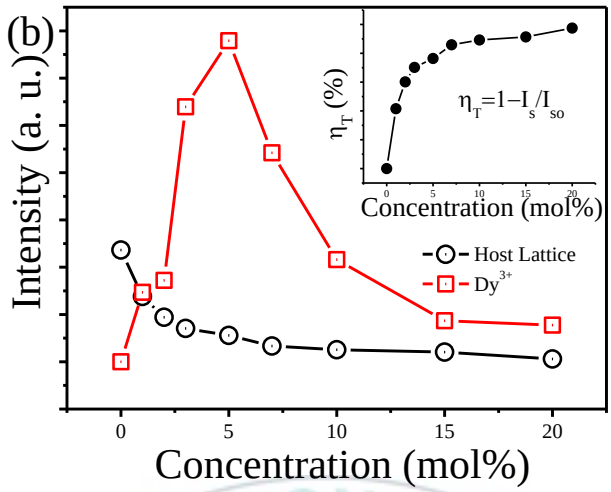

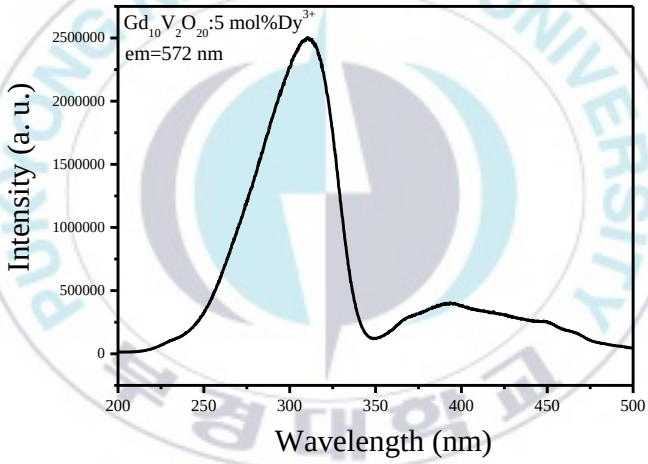

Figure 2-8 (a) PL spectra of the $Gd_{10}V_2O_{20}$:*x* Dy^{3+} (*x* = 0, 0.01, 0.02, 0.03, 0.05, 0.07, 0.1, 0.15, 0.2, 0.3, 0.5 and 0.7) phosphors (λ*ex* = 266 nm), (b) calculated emission intensities of the host lattice and Dy^{3+} ions at different Dy^{3+} doping concentration, (c) PLE spectra of the $Gd_{10}V_2O_{20}$:5 mol% Dy^{3+}

Figure 2-8 (a) shows the PL spectra of Dy^{3+}-activated $Gd_{10}V_2O_{20}$ phosphors at different Dy^{3+} concentrations. With the excitation at 266 nm, a broad band centered at 455 nm can be observed in pure phosphor. After doping Dy^{3+} into the

lattice, two emission peaks at 483 and 575 nm which originate from the $^4F_{9/2}\rightarrow{}^6H_{15/2}$ (blue emission) and $^4F_{9/2}\rightarrow{}^6H_{13/2}$ (yellow-green emission) transitions of Dy^{3+} ions can be found. With increasing the Dy^{3+} ion concentration, the intensity of Dy^{3+} emissions increases gradually and reaches its maximum value at point x=0.05. Then, the intensity decreases with further increasing the Dy^{3+} concentration owing to the concentration quenching caused by the resonant ET between Dy^{3+} ions. However, the host emission decreases gradually with increasing the Dy^{3+} concentration due to the energy transfer from host to the Dy^{3+} ions, as shown in Figure 2-8 (b)[22-24].

The PLE spectra of $Gd_{10}V_2O_{20}$:5 mol% Dy^{3+} samples are shown in Figure 2-8 (c), illustrates a broad charge transfer band centered at 310 nm from 240 to 350 nm. The broad band can be ascribed to a charge transfer from VO_4^{2-} group to Dy^{3+}.

2.3.3. Temperature dependent properties of the Dy^{3+}-activated $Gd_{10}V_2O_{20}$ phosphors

An important parameter for phosphors is the luminescence quenching on temperature since the luminescence materials may work at different environment, or suffer from hard temperatures during the preparation of the devices. Comprehensive understanding of the temperature dependent deterioration and quenching should be beneficial to the improvement of the phosphor performance by the material design.

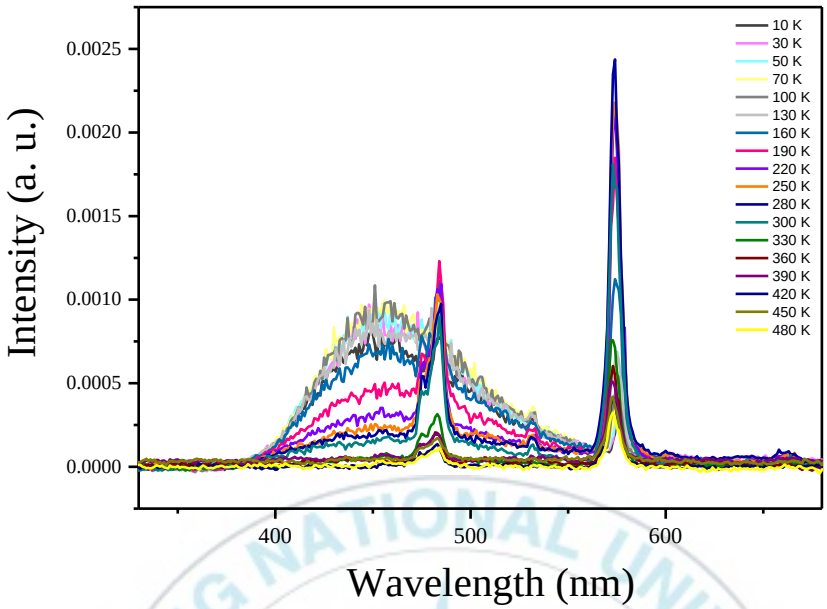

Figure 2-9 Temperature dependent emission spectra of emission spectra (λex = 266 nm) of the $Gd_{9.99}V_2O_{20}$: 1.0 mol% Dy^{3+} sample

Figure 2-9 shows the temperature dependent emission spectra of the $Gd_{9.99}V_2O_{20}$: 1.0 mol% Dy^{3+} in the region of 330~680 nm under the excitation of 266 nm in the temperature range from 10 K to 480 K. The emission spectra exhibit broad band with the maxima at around 455 nm together with sharp lines. The broad band emission is due to the charge transfer transition from the 2p orbital of the O^{2-} ligand to the 5d orbital of the d^0 vanadium metal ion. And the line emissions at 483 nm and 573 nm can be ascribed to the Dy^{3+} $^4F_{9/2}\rightarrow{}^6H_{15/2}$ and $^4F_{9/2}\rightarrow{}^6H_{13/2}$ transitions respectively[35-36]. With the increase of temperature, the broad band emission is quenched due to the energy transfer and thermal quenching effect. The emission intensity of Dy^{3+} increases firstly due to the increase of the energy transfer rate from 10 K to 300 K and then decreases due to the thermal quenching effect.

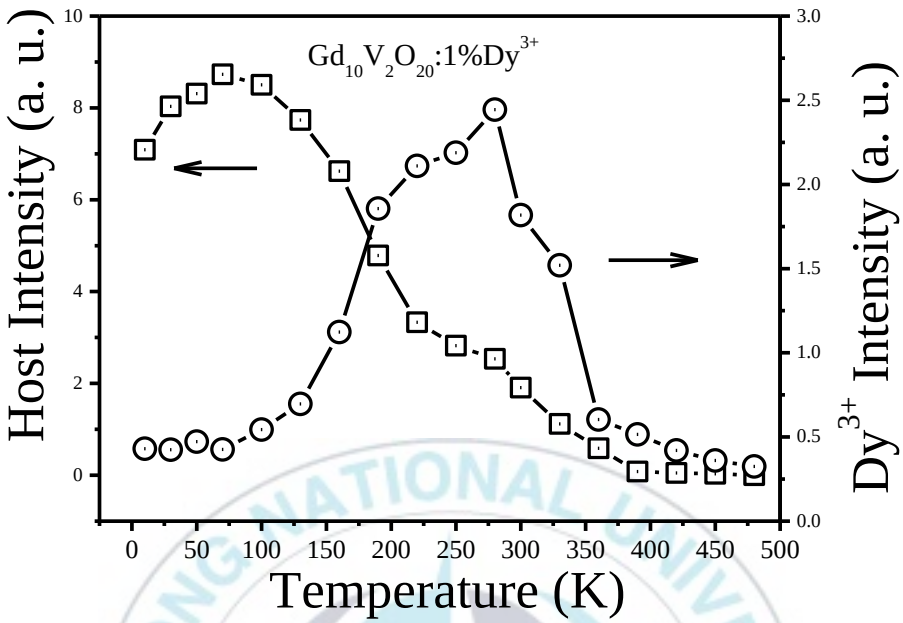

Figure 2-10 Calculated integral emission intensity of the vanadate group and Dy^{3+} emission band.

To further study the temperature dependent photoluminescence performance, the calculated integral emission intensity of vanadate group and Dy^{3+} emission intensity of the $Gd_{9.99}V_2O_{20}$: 1.0 mol% Dy^{3+} samples are investigated in the temperature range from 10K to 480 K, as shown in Figure 2-10. The emission intensity of vanadate group increases with the increase of temperature, the maximum emission intensity of vanadate group appears at x = 70 K, when the temperature is higher above 70 K, the emission intensity of vanadate group decreases due to the energy transfer and thermal quenching effect. At low temperature, the Dy^{3+} emission intensity increases with increasing temperature and reaches maximum at room temperature. Above the room temperature, the Dy^{3+} emission intensity decreases with the increase of temperature which is due

to thermal quenching effect.

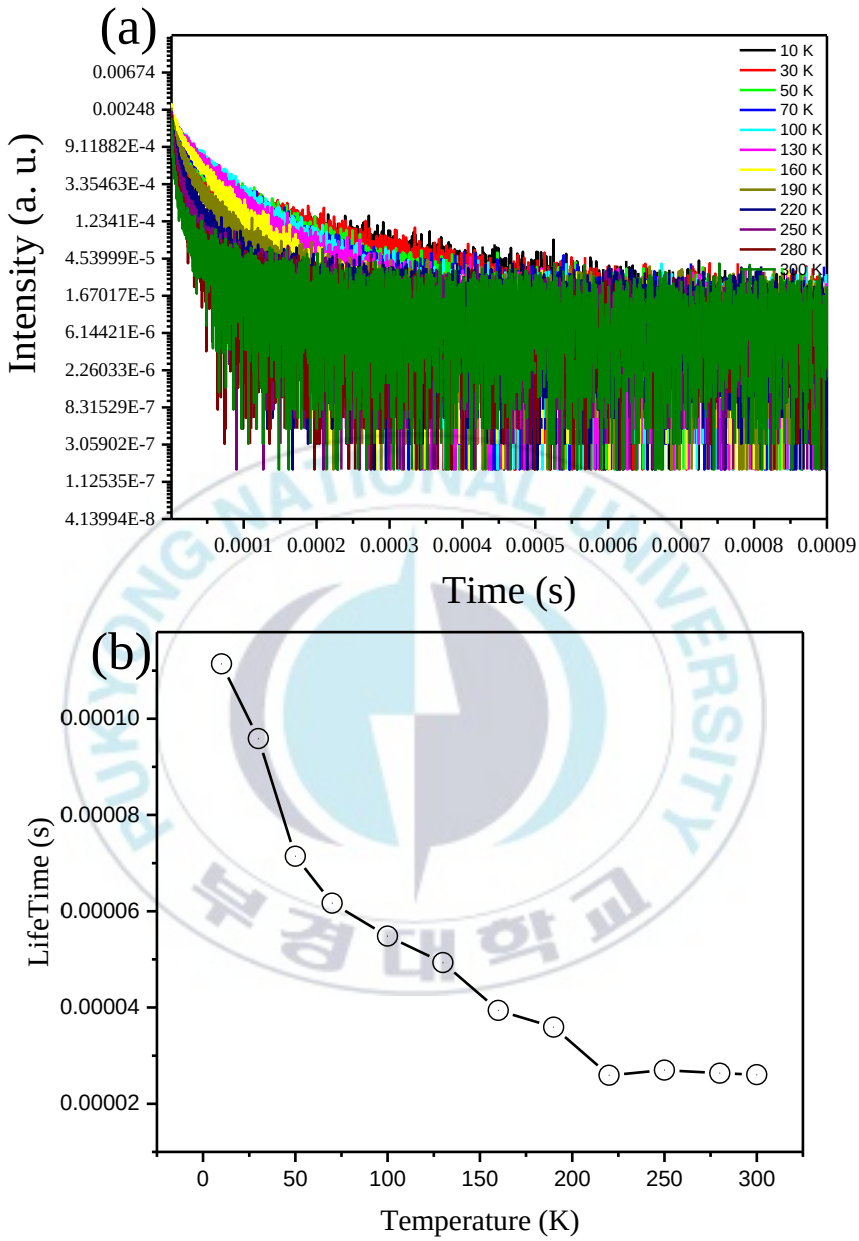

Figure 2-11 (a)The decay curves (λex = 266 nm) (λem = 421 nm) the $Gd_{9.99}V_2O_{20}$: 1.0 mol% Dy^{3+} sample and (b)calculated lifetime of phosphors with different low-temperature dependent

Figure 2-11 (a) is the decay curves at 421 nm of the $Gd_{9.99}V_2O_{20}$: 1.0 mol%

Dy^{3+} under the excitation of 266 nm with different temperature from 10K to 300K. The lifetime decreases with the increasing of temperature and also decreases with the increasing of Dy^{3+} ions doping concentration. The calculated lifetimes with a different temperature for the $Gd_{9.99}V_2O_{20}$: 1.0 mol% Dy^{3+} samples were displayed in Figure 2-11 (b).

3. Synthesis and Luminescence properties of 5mol%Dy^{3+}, *x* Sm^{3+}-activated doped $Gd_{10}V_2O_{20}$

3.1. Introduction

Under the excitation of ultraviolet light, white light can be obtained by single doped Dy^{3+}. The two main emission bands of Dy^{3+} are located at blue light region 460–500 nm ($^4F_{9/2} \rightarrow {}^6H_{15/2}$) and yellow light region 550–600 nm ($^4F_{9/2} \rightarrow {}^6H_{13/2}$)[25]. There is also the same problem in this combination of blue and yellow, which is the lack of red light. Co-doped Sm^{3+} can be used to supplement the emission of the red light region, because of Sm^{3+} $^4G_{5/2} \rightarrow {}^6H_{J/2}$ (J = 5, 7, 9) emissions in the orange-red region. However, the Sm^{3+} ion has weak absorption in the UV region[26]. Only a few articles have been reported on Dy^{3+} and Sm^{3+} co-doped phosphors[27-31]. Energy transfer is often found in the multi-doped phosphors, such as $Dy^{3+} \rightarrow Sm^{3+}$[27-31], $Ce^{3+} \rightarrow Tb^{3+}$[32], $Eu^{2+} \rightarrow Mn^{2+}$[33], and $Eu^{2+} \rightarrow Tb^{3+} \rightarrow Sm^{3+}$[34]. Dy^{3+} can transfer energy to Sm^{3+}, because there is an overlap between the emission spectrum of Dy^{3+} and the excitation spectrum of Sm^{3+} as well as excited state of Dy^{3+} ($^4F_{9/2}$) slightly higher than that of Sm^{3+} ($^4I_{19/2}$).

In this paper, the Dy^{3+} and Sm^{3+}activated $Gd_{10}V_2O_{20}$ phosphors were synthesized by the high-temperature solid-state method. The photo-luminescence (PL) properties, ET mechanism between Dy^{3+} and Sm^{3+} ions in $Gd_{10}V_2O_{20}$ phosphors, and chromatic properties were investigated.

3.2. Experimental Section

3.2.1. Sample preparation

5mol%Dy^{3+},*x* Sm^{3+} doped $Gd_{10}V_2O_{20}$ doped $Gd_{10}V_2O_{20}$ with various Sm^{3+} concentrations of *x*=0.01, 0.03, 0.05, 0.1 were synthesized via the high-temperature solid-state method. The specific operation steps are as follows:

A．Raw material is weighted

Turn on the electronic balance and preheat for a few minutes, after the electronic balance is stabilized, according to the appropriate stoichiometric ratio, the starting materials, Gd_2O_3 (Aldrich, 99.9%), V_2O_5 (Aldrich, 99.9%), Dy_2O_3 (Aldrich, 99.9%)，Sm_2O_3 (Aldrich, 99.9%).

B．mixture the starting materials

All the starting reagents were mixed in stoichiometric ratios and ground in an agate mortar to obtain the homogeneous mixture.

C．Previous calcining

Starting reagents were grounded thoroughly in an agate mortar with ethanol, the mixture was calcined at 600 ℃ for 6 h in a crucible in the atmosphere, and then cooling to room temperature.

D. Ground and calcinate again

After cooling to room temperature, grounded thoroughly again in an agate mortar with ethanol, then the homogenous mixture was calcined at 1200 ℃ for 12 h in a crucible in the atmosphere. Thus, a series of the 5mol%Dy^{3+},*x* Sm^{3+} doped $Gd_{10}V_2O_{20}$ phosphors were successfully obtained as cooling down to room temperature.

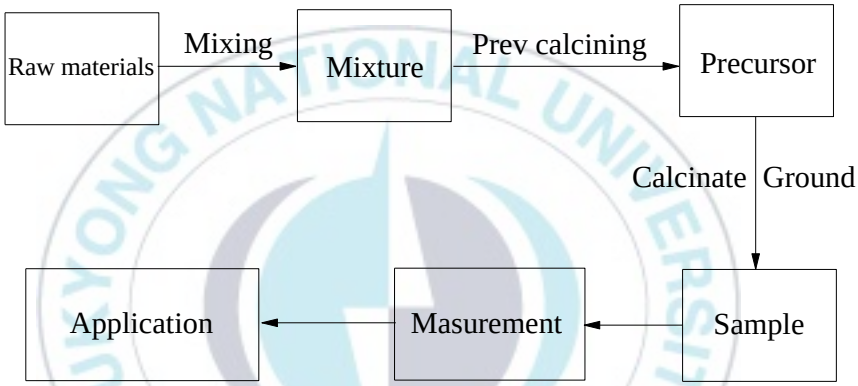

Figure 3-1 The preparation process of the high-temperature solid-state method

3.2.2. Characterization

In this work, the crystal phases of the 5mol%Dy^{3+},*x* Sm^{3+} doped $Gd_{10}V_2O_{20}$ samples were identified by using an X-ray Rigaku D/Max diffractometer(XRD) operating at 40 kV, 30 mA equipped by Cu *K*α radiation (λ= 1.5405 Å). A 450 W Xe lamp dispersed by a 25 cm monochromator (Acton Research Corp. Pro-250) was used as a light source for excitation and emission spectra. The luminescence

signal was detected using a photomultiplier tube (PMT) (Hamamatsu, R928, Shizuoka, Japan) mounted on a 75 cm monochromator (Acton Research Corp. Pro-750). The third harmonic (266 nm) of a pulsed Nd: YAG laser was introduced as an excitation source for luminescence decays which were digitized and saved by means of a 500 MHz Tektronix DPO 3054 oscilloscope.

3.3. Results and Discussion

3.3.1. Structure, morphology and composition

Figure 3-2 shows the XRD patterns of 5mol%Dy^{3+},*x* Sm^{3+} doped $Gd_{10}V_2O_{20}$ (*x*=0.01, 0.03, 0.05, 0.1) samples synthesized by high-temperature solid-state reaction method. Which are well indexed to the standard card (PDF # 22-0296) without any impurities phases. No evident peak shift in the XRD patterns is observed even at Sm^{3+} content of 10 mol% indicating the introduction of activated 5mol%Dy^{3+},*x* Sm^{3+} impurities do not cause significant changes to the crystallinity.

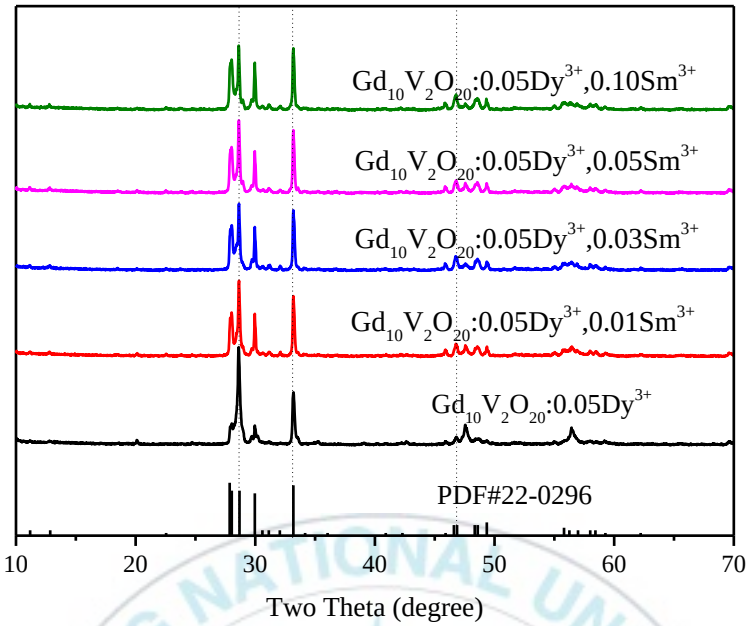

Figure 3-2 XRD patterns of $Gd_{9.95-x}V_2O_{20}$:5% Dy^{3+}, x%Sm^{3+} and $Gd_{9.95}V_2O_{20}$:5% Dy^{3+} phosphors.

The PL emission spectra of 5mol%Dy^{3+}, $x$$Sm^{3+}$ doped $Gd_{10}V_2O_{20}$ phosphors for different Sm^{3+} ion concentrations at an excitation wavelength of 266 nm, Figure 3-3 shows four strong emission peaks a 483, 575, 600, and 647 nm, which corresponds to the $^4F_{9/2} \rightarrow {}^6H_{15/2}$, $^4F_{9/2} \rightarrow {}^6H_{13/2}$, $^4G_{5/2} \rightarrow {}^6H_{7/2}$, and $^4G_{5/2} \rightarrow {}^6H_{9/2}$ transitions of Sm^{3+}, respectively. With the increasing of Sm^{3+} concentration, the luminescence intensity increased first and then decreased, and the optimum concentration is x = 0.05.

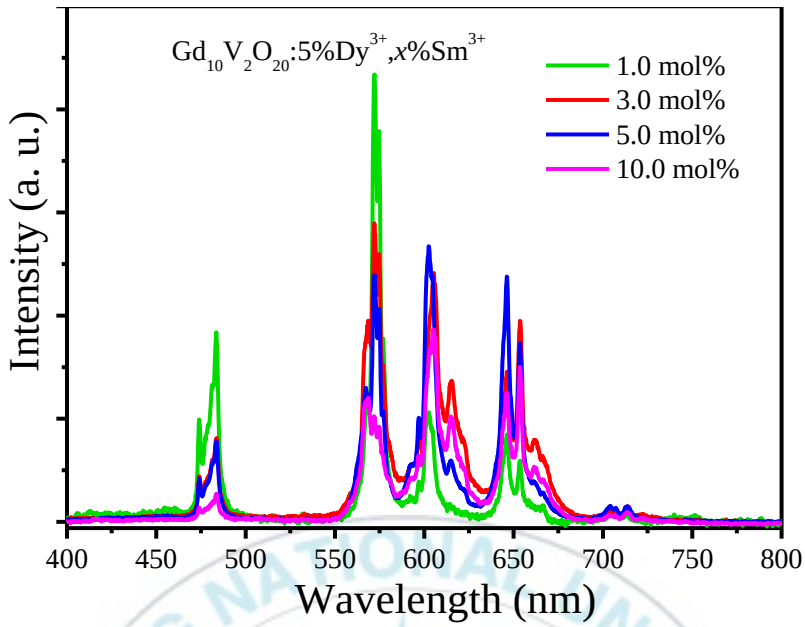

Figure 3-3 Emission spectra of $Gd_{9.95-x}V_2O_{20}$: 5mol%Dy^{3+}, $x$$Sm^{3+}$ phosphors

To further confirm the energy transfer from 5mol%Dy^{3+}, $x$$Sm^{3+}$ doped $Gd_{10}V_2O_{20}$ phosphors, the emission spectra of $Gd_{9.95-x}V_2O_{20}$: 5mol%Dy^{3+}, $x$$Sm^{3+}$ and the decay curves of $Gd_{9.95-x}V_2O_{20}$: 5mol%Dy^{3+}, $x$$Sm^{3+}$ were investigated. Under the excitation at 352 nm, the emission spectra of $Gd_{9.95-x}V_2O_{20}$: 5mol%Dy^{3+}, $x$$Sm^{3+}$ (x = 0.01, 0.03, 0.05 and 0.1) are shown in Figure 3-3, which originate from the $^4G_{5/2} \rightarrow {}^6H_{9/2}$ transition of Sm^{3+} ion. When the Sm^{3+} concentration is 0.05, it can be observed that the intensity of emission peak achieves highest. Then, with the increase of Sm^{3+} concentration, the luminous intensity gradually decreases. The lifetime decay curves of $Gd_{9.95-x}V_2O_{20}$: 5mol%Dy^{3+}, $x$$Sm^{3+}$ (x = 0.01, 0.03, 0.05 and 0.1) monitored at 573 nm and 605 nm are depicted in Figure 3-4 and Figure 3-5. The decay curves are analyzed based on the following double-exponential equation:

$$I(t) = I_0 + \exp(-t/\tau_1) + A_2\exp(-t/\tau_2) \quad (3\text{-}1)$$

Where I and I_0 are the luminescence intensities at time t and 0, A_1 and A_2 are fitting parameters, and τ_1 and τ_2 are lifetimes for exponential components, respectively. The average lifetime could be evaluated by the following equation:

$$\tau = \frac{(A_1\tau_1^2 + A_2\tau_2^2)}{(A_1\tau_1 + A_2\tau_2)} \quad (3\text{-}2)$$

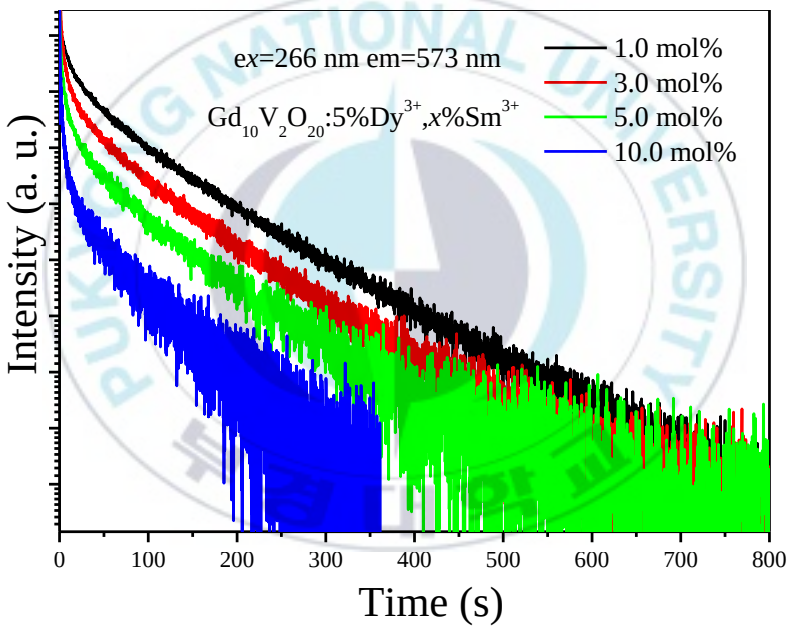

Figure 3-4 Decay curves of $Gd_{9.95-X}V_2O_{20}$:5% Dy^{3+}, x%Sm^{3+} at 573 nm.

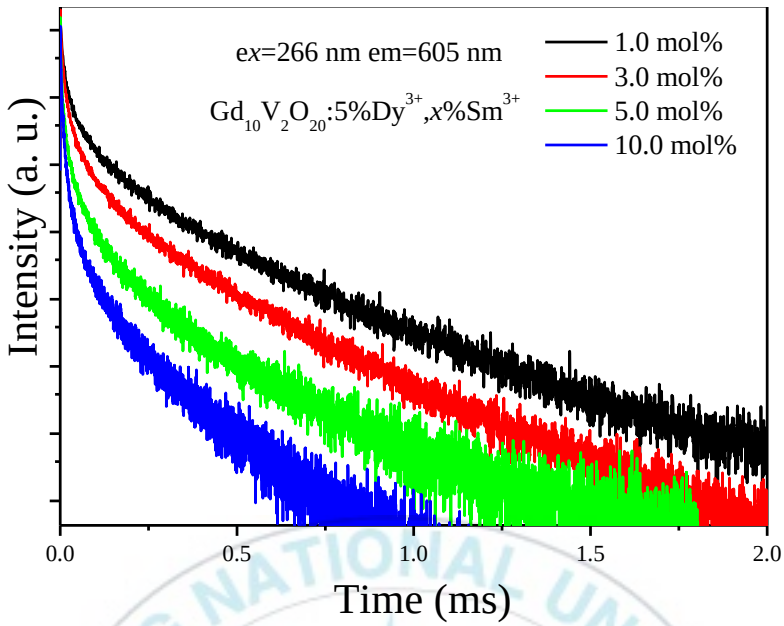

Figure 3-5 Decay curves of $Gd_{9.95-x}V_2O_{20}$:5% Dy^{3+}, x%Sm^{3+} phosphors at 605 nm.

The fitting results τ calculated by equation (2) are 140, 105, 99 and 58 ms for 5mol%Dy^{3+}, $x$$Sm^{3+}$ doped $Gd_{9.95-x}V_2O_{20}$ (x = 0.01, 0.03, 0.05 and 0.1) respectively. With the increase of Sm^{3+} concentration, the decay times of 5mol%Dy^{3+}, $x$$Sm^{3+}$ doped $Gd_{9.95-x}V_2O_{20}$ decrease gradually. All these results provide evidence for the energy transfer from Dy^{3+} to Sm^{3+} in the $Gd_{10}V_2O_{20}$ host.

3.3.2. Energy transfer

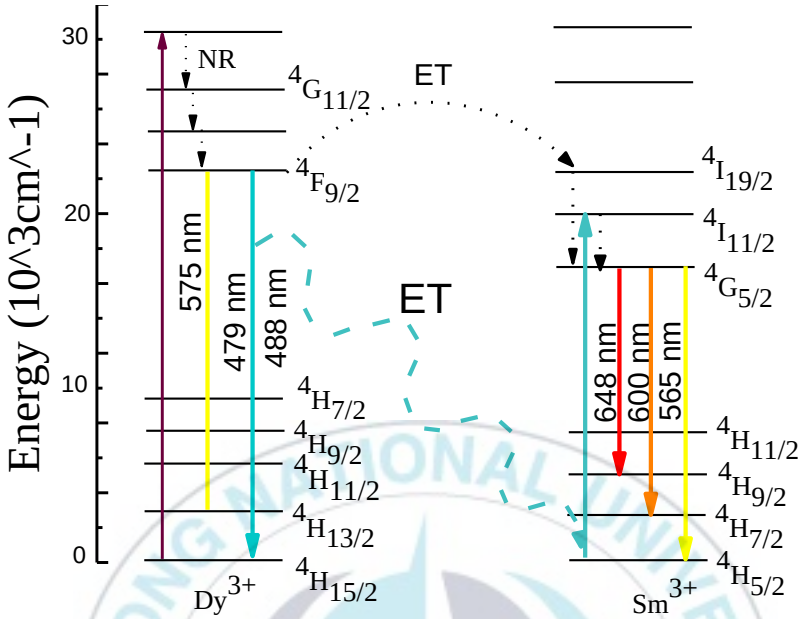

Figure 3-6 The schematic diagram of energy transfer

Figure 3-6 gives the schematic diagram of energy transfer from 5mol%Dy^{3+}, xSm^{3+} doped $Gd_{10}V_2O_{20}$ (x = 0.01, 0.03, 0.05 and 0.1). It can be seen that the excited state of Dy^{3+} ($^4F_{9/2}$) slightly higher than that of Sm^{3+} ($^4I_{19/2}$), which means energy transfer can occur through the non-radiative process. The radiative way of energy transfer is due to the spectral overlap of the Sm^{3+} excitation and the Dy^{3+} emission[38].

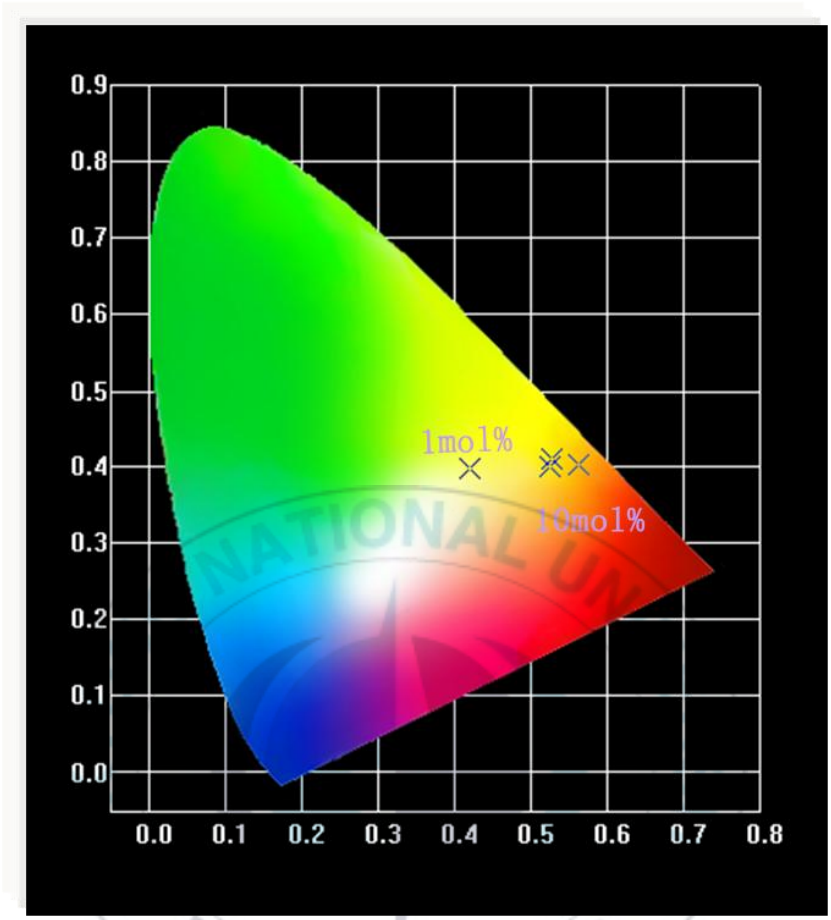

Figure 3-7 The CIE chromaticity diagram of $Gd_{9.95-x}V_2O_{20}$:5% Dy^{3+}, x%Sm^{3+} (x = 0-10).

In Figure 3-7 Commission International de L'Eclairage (CIE) diagram shows emission color of the 5mol%Dy^{3+}, $x$$Sm^{3+}$ doped $Gd_{10}V_2O_{20}$ (x = 0.01, 0.03, 0.05 and 0.1) sample can be turned from the yellow to the red region with the increase of Sm^{3+} doping concentration.

4. Conclusion and acknowledgment

4.1. Conclusion

In this work, a series of Dy^{3+} co-doped $Gd_{10}V_2O_{20}$ is synthesized by the conventional high-temperature solid-state method. And their photoluminescence properties were investigated deeply.

Concentration-dependent excitation spectra, emission spectra, fluorescence color, and lifetime decay curves were measured and the optimum doping concentration of Dy^{3+} co-doped $Gd_{10}V_2O_{20}$ lattice was 3mol%.

Relative and absolute sensitivities of Dy^{3+} co-doped $Gd_{10}V_2O_{20}$ are temperature dependent under the 266 nm excitation in the temperature range from 10 K to 480 K are investigated.

Dy^{3+} and Sm^{3+}activated $Gd_{10}V_2O_{20}$ phosphors were synthesized by the high-temperature solid-state method. The photo-luminescence (PL) properties, ET mechanism between Dy^{3+} and Sm^{3+} ions in $Gd_{10}V_2O_{20}$ phosphors, and chromatic properties were investigated.

4.2. Acknowledgments

Foremost, I would like to express my sincere gratitude to my advisor Prof. Hyo Jin Seo, under for his kind behavior, constant attention, valuable suggestions, encouraging altitude His guidance has helped me a lot during the last two years of research and living in South Korea.

I would like to thank some Chinese professors. Especially thanks to Prof.

Yan-Lin Huang from Soochow University who gave me advice and helped during the past two years.

Thanks to my lab-mates. Donglei Wei, Lin Qin, Cuili Chen, Jing Wang, Zutao Fan, et al., for their conceptual discussion, for the span we spent together in the research group.

At last, I also want to dedicate this work to my parents and my older brother. Thank all my relatives for their endless care and understanding of my study. You are my biggest spiritual support. I wish you happiness, health, and happiness forever.

5. References

[1] K. N. Shinde, S. J. Dhoble, Critical Reviews in Solid State and Materials Sciences 39(6) (2014) 459-479.

[2] G. Blasse, B. C. Grabmaier, Luminescent Materials [M]. Berlin Heidelberg: Springer-Verlag (1994) 10-32.

[3] N. Holonyak Jr, S. Bevacqua, Applied Physics Letters 1 (1962) 82.

[4] S.W. Kaun, E. Ahmadi, B. Mazumder, F. Wu, E.C. Kyle, P.G. Burke, U.K. Mishra, J.S. Speck, Semiconductor Science and Technology 29 (2014) 045011.

[5] D. C. Harris, M. D. Bertolucci, Courier Corporation (1989).

[6] X. Wang, R. R. Valiev, T. Y. Ohulchanskyy, Chemical Society Reviews 46(14) (2017) 4150-4167.

[7] F. Wang, Y. Han, C. S. Lim, nature 463(7284) (2010) 1061.

[8] Y. Guo, B. K. Moon, B. C. Choi, et al. RSC Advances 7(37) (2017) 23083-23092.

[9] J. C. G. Bünzli, C. Piguet, Chemical Society Reviews 34(12) (2005) 1048-1077.

[10] G. Blasse, B. C. Grabmaier, Luminescent materials (1994) 10-32

[11] F. Yang, H. Ma, Y. Liuc, B. Han, H. Feng, Q. Yu, Ceramics International 40 (2014) 10189-10192.

[12] C. H. Liang, L. G. Teoh, K. T. Liu, Y. S. Chang, Journal of Alloys and Compounds 517 (2012) 9-13.

[13] J. Y. Wang, J. B. Wang, P. Duan, Materials Letters 107 (2013) 96-98.

[14] Q. Liu, Y. Liu, Y. Ding, Z. Peng, X. Tian, Q. Yu, G. Dong, Ceramics International 40 (2014) 10125-10129.

[15] R. Shrivastava, J. Kaur, V. Dubey, Journal of fluorescence 26(1) (2016) 105-111.

[16] J. Kuang, Y. Liu, J. Zhang, The Journal of Physical Chemistry 179(1) (2006) 266-269.

[17] D. V. Sunitha, H. Nagabhushana, S. C. Sharma, B. M. Nagabhushana, B. D. Prasad, R. P. S. Chakradhar, Spectrochim. Spectrochimica Acta Part A: Molecular and Biomolecular Spectroscopy 127 (2014) 381-387.

[18] L. Lin, Z. Zhao, W. Zhang, Z. Zheng, M. Yin, Journal of Rare Earths 27(5) (2009) 749-752.

[19] P. Du, L. K. Bharat, X. Y. Guan, J. S. Yu, Journal of Applied Physics 117(8) (2015) 083112.

[20] Y. Tian, B. Chen, B. Tian, Journal of alloys and compounds 509(20) (2011) 6096-6101.

[21] J. Zhao, C. Guo, X. Su, H. M. Noh, J. H. Jeong, Journal of the American Ceramic Society 97(6) (2014) 1878-1882.

[22] V. Bedekar, D. P. Dutta, M. Mohapatra, S. Godbole, R. Ghildiyal, A. Tyagi, Nanotechnology 20(12) (2009) 125707.

[23] P. H. Yang, X. Yu, X. H. Xu, T. M. Jiang, H. L. Yu, D. C. Zhou, Z. W. Yang, Z. G. Song, J. B. Qiu, Journal of Solid State Chemistry 202 (2013) 143-148.

[24] M. Yu, J. Lin, Z. Wang, J. Fu, S. Wang, H. J. Zhang, Y. C. Han, Chemistry of Materials 14(5) (2002) 2224-2231.

[25] D. P. Dutta, R. Ghildiyal, A. K. Tyagi,. The Journal of Physical Chemistry C 113(39) (2009) 16954-16961.

[26] H. Guan, C. Xu, Y. Sheng, The Journal of Physical Chemistry C 121(12) (2017) 6884-6897.

[27] D. Balaji, K. Kavirasu, A. Durairajan, Journal of Alloys and Compounds 637 (2015) 350-360.

[28] X. Zhang, H. J. Seo, Journal of Alloys and Compounds 509(5) (2011) 2007-2010.

[29] G. S. R. Raju, S. Buddhudu, Spectrochimica Acta Part A: Molecular and Biomolecular Spectroscopy 70(3) (2008) 601-605.

[30] D. Balaji, K. Kavirasu, A. Durairajan, Journal of Alloys and Compounds 637 (2015) 350-360.

[31] X. Li, X. Wang, Physica B: Condensed Matter 481 (2016) 197-203.

[32] Z. Xia, R. S. Liu, The Journal of Physical Chemistry C 116(29) (2012) 15604-15609.

[33] N. Guo, Y. Huang, H. You, Inorganic chemistry 49(23) (2010) 10907-10913.

[34] J. Sun, X. Zhang, Z. Xia, Journal of Applied Physics 111(1) (2012) 013101.

[35] L. Lin, M. Yin, C. Shi, W. Zhang, Journal of Alloys and Compounds 455 (2008) 327.

[36] A. A. Reddy, M. C. Sekhar, K. Pradeesh, S. S. Babu, G. V. Prakash, Journal of Materials Science 46 (2011) 2018

[37] D. P. Dutta, R. Ghildiyal, A. K. Tyagi,. The Journal of Physical Chemistry C

113(39) (2009) 16954-16961.

[38] H. Wu, Z. Sun, S. Gan, L. Li, Solid State Sciences 85 (2018) 48-53.